Steel and Composite Structures, *Vol. 39, No. 5 (2021) 543-564*
DOI: https://doi.org/10.12989/scs.2020.39.5.543

Investigating the effect of edge crack on the modal properties of composite wing using dynamic stiffness matrix

Ali Reza Torabi[1], Shahrokh Shams*[2] and Mahdi Fatehi-Narab[2]

[1]*Fracture Research Laboratory, Faculty of New Science and Technologies, University of Tehran, Tehran, Iran*
[2]*Faculty of New Sciences and Technologies, University of Tehran, Tehran, Iran, P.C:1439957131*

(*Received January 15, 2020, Revised April 16, 2021, Accepted April 20, 2021*)

Abstract. In this study free vibration analysis of a cracked Goland composite wing is investigated. The wing is modelled as a cantilevered beam based on Euler- Bernoulli equations. Also, composite material is modelled based on lamina fiber-reinforced. Edge crack is modelled by additional boundary conditions and local flexibility matrix in crack location, Castigliano's theorem and energy release rate formulation. Governing differential equations are extracted by Hamilton's principle. Using the separation of variables method, general solution in the normalized form for bending and torsion deflection is achieved then expressions for the cross-sectional rotation, the bending moment, the shear force and the torsional moment for the cantilevered beam are obtained. The cracked beam is modelled by separation of beam into two interconnected intact beams. Free vibration analysis of the beam is performed by applying boundary conditions at the fixed end, the free end, continuity conditions in the crack location of the beam and dynamic stiffness matrix determinant. Also, the effects of various parameters such as length and location of crack and fiber angle on natural frequencies and mode shapes are studied. Modal analysis results illustrate that natural frequencies and mode shapes are affected by depth and location of edge crack and coupling parameter.

Keywords: cracked wing; dynamic stiffness matrix; two interconnected Euler–Bernoulli beams

1. Introduction

Industries to save weight and for tailoring materials properties according to the design requirements (Shiau 1992, Shu and Della 2004). Moreover, fiber-reinforced composite materials also suffer from damages. These damages may occur as a consequence of defects introduced during the manufacturing process or it may result from external loads occurring during the operational life such as impact by foreign objects (Shen and Grady 1992). In fact, defects lead to damage and damages lead to failure in structure and finally failure in the structure leads to mishap (Worden and Barton 2004). Therefore damage detection in these materials is quite important. In this field, one important method is structural health monitoring (SHM) based on vibration properties. The premise of this method is that damage will alter the stiffness, mass or damping properties of a structure which in turn affects the dynamic response of the structure such as natural frequencies, mode shapes and damping ratio of the structure (Wang *et al.* 2005). Also, free vibration analysis is a prerequisite for other analyses as aero-elastic analysis. So, more attention should be paid to modal analysis of damaged composite structures. Commonly for vibration analysis of airplane components, they can be idealized as engineering elements such as shell, plate and beam. Most of engineering components can be idealized as cantilevered beams for example high aspect ratio wings, helicopter blades, airplane propellers, turbine vanes and windmill turbines. Free vibration analysis of these components will be important for understanding of mechanical behavior and reliability of structure.

In recent years, numerous studies have been performed in the field of free vibration analysis fields of composite structures. Weisshaar and Foist (1985) discussed free-vibration characteristics of directionally stiffened, laminated composite beam-like structures such as high-aspect-ratio lifting surfaces. Hodges *et al.* (1991) generated methods for predicting the natural frequencies and mode shapes of composite beams. Song and Librescu (1991) analysed the free vibration and aero-elastic divergence of aircraft wings modelled as thin-walled anisotropic. Also a semi analytical method is employed to obtain the buckling loads and the natural frequencies of symmetric cross-ply laminated composite plates with edges elastically restrained against both translation and rotation by Ashour (2003). Banerjee and Williams (1995) used a dynamic stiffness matrix method to predict the free vibration characteristics of composite beams for coupled (materially) bending and torsional displacements. Banerjee (2001) designed a systematic procedure for derivation of exact expressions for the frequency equation and mode shapes of composite beams undergoing free vibration. Banerjee *et al.* (2008) considered a dynamic stiffness matrix of a composite beam that exhibits both geometric and material coupling between bending and torsional motion and investigates its free vibration characteristics. Then, the Wittrick–Williams algorithm is applied to find the dynamic stiffness matrix, the natural frequencies and mode shapes of an illustrative example. Also, the dynamic stiffness formulation for both in-plane

*Corresponding author, Mr.
E-mail: shahrokh.shams@ut.ac.ir

ISSN: 1229-9367 (Print), 1598-6233 (Online)

and bending free vibration based on the first order shear deformation theory for composite plates were presented by Boscolo and Banerjee (2012). The exact solutions for the spatially coupled free vibration analysis of composite box beams resting on elastic foundation under the axial force using the power series method based on the homogeneous form of simultaneous ordinary differential equations and dynamic stiffness matrix are presented by Kim (2009). Chronopoulos *et al.* (2013) proposed a dynamic stiffness approach for the prediction of the vibratory response of thick laminates and sandwich panels. The procedures and results of a modal test for a honeycomb sandwich panel for aerospace applications are presented and discussed by Sousa *et al.* (2016).

But fewer investigates have been performed in the field of free vibration analysis of damaged composite structures. Free vibration and damping characteristics of composite beams with holes are investigated experimentally and numerically by Demir (2016). Krawczuk and Ostachowicz (1995) investigated the eigen-frequencies of a cantilever beam made from graphite-fiber reinforced polyimide with a transverse one-edge non-propagating open crack, then they investigated the discrete-continuous and finite element (FE) model of a composite beam with a transverse one-edge non-propagating open crack. Strganac and Kim (1996) studied the aero-elastic response of several damaged composite plates and developed a model of microstructural damage. Then they presented two examples of aero-elastic systems with microstructural damage: 1) a panel flutter of a composite plate and 2) a bending-torsion flutter of a wing represented by a cantilevered composite. Song and Librescu (2003) developed an exact solution method based on Laplace transform technique enabling one to analyse the bending free vibration of cantilevered laminated composite beams weakened by multiple non-propagating part-through surface cracks. Also, Wang *et al.* (2005) investigated aero-elastic characteristics of a cantilevered composite panel of large aspect ratio with an edge crack. They modelled a one-dimensional beam vibrating in coupled bending and torsion and revealed that edge crack does not necessarily reduce either flutter or divergence speed because the critical speeds are also affected by the bending-torsion coupling parameter due to the material. In another work, Wang and Inman (2007) studied crack-induced changes in the aero-elastic boundaries of an un-swept composite wing. The bending- torsion couplings are applied to the equation of motion due to the unbalanced laminates and offset of the centre of gravity. The edge crack which is modelled with the local flexibility concept, introduces additional boundary conditions at the crack location. Daneshmehr *et al.* (2013) considered free vibration of cracked composite beams subjected to coupled bending-torsion loading based on a first order theory to study the influence of open edge cracks on first natural frequency of the beam. Jafari (2015) investigated the free vibration analysis of rotating delaminated composite beams with general lay-ups using an assumed series solution in conjunction with Lagrange multipliers. This paper illustrates that the present method has a rapid convergence properties in predicting the natural frequencies and mode shapes of the beams.

The current study is motivated by Banerjee *et al.* (2008) and Wang and Inman (2007) studies which are concerned with the dynamic stiffness formulation and free vibration analysis of composite cracked beams that exhibit bending–torsion coupling. The current paper relies on one frequency dependent matrix called the dynamic stiffness matrix which has mass and stiffness properties of the structure together, unlike other methods such as FEM that relies on two separate matrices, mass and stiffness matrices (Banerjee and Su 2006). In this paper crack effects on the modal characteristics of composite Goland wing are studied and damage effects on the natural frequencies are illustrated. Also in this study, free vibration analysis of an intact composite beam is considered and its results are verified with similar works. Then free vibration analysis of cracked Goland composite beam is determined. The contribution of this study is compared to previous works regarding both geometric and material coupling in cracked Goland wing modelling and use of formulations and approaches related to dynamic stiffness matrix. The originality of the presented study is notable from two points of view. From method and formulation point of view in comparison with Banerjee *et al.* (2008) including edge crack effects and in comparison with Wang and Inman (2007) using dynamic stiffness matrix method including both geometric and material coupling. This study is quite new compared with the previous ones from the results and analyses point of view. Thus, the novelty of this study is to develop the dynamic stiffness matrix method for free vibration analysis of cracked wing with including coupling parameters.

2. Governing equations

The wing is idealized as a bending-torsion coupled cantilevered beam with negligible damping. Since structural damping of the wing model is negligible in comparison with other structural parameters e.g. stiffness and mass of the structure and in the aero-elastic analysis, contribution of structural damping is small in comparison with aerodynamic damping (Ling *et al.* 2015) and also to reduce the complexity, here damping is neglected.

The model is illustrated in Fig. 1 represents a cantilevered wing with a span length L, chord length b, crack length a, fiber angle θ and principle axes which is specified by 1 and 2. Also in this model x_α is the distance between the mass and elastic axes, which is responsible for geometric coupling.

According to Meirovitch and Silverberg (1984), Banerjee (2001) and Wang (2004), by utilizing bending-torsion material coupling rigidity term and assuming that cross section is non-variable, the following governing differential equations are obtained

$$\begin{aligned} EI\frac{d^2}{dy^2}\left(\frac{d^2\mathrm{h}}{dy^2}\right) - K\frac{d}{dy}\left(\frac{d^2\psi}{dy^2}\right) + m\frac{d^2\mathrm{h}}{dt^2} + mx_\alpha\frac{d^2\psi}{dt^2} = 0, \\ GJ\frac{d^2\psi}{dy^2} - K\frac{d}{dy}\left(\frac{d^2\mathrm{h}}{dy^2}\right) - mx_\alpha\frac{d^2\mathrm{h}}{dt^2} - I_\alpha\frac{d^2\psi}{dt^2} = 0. \end{aligned} \quad (1)$$

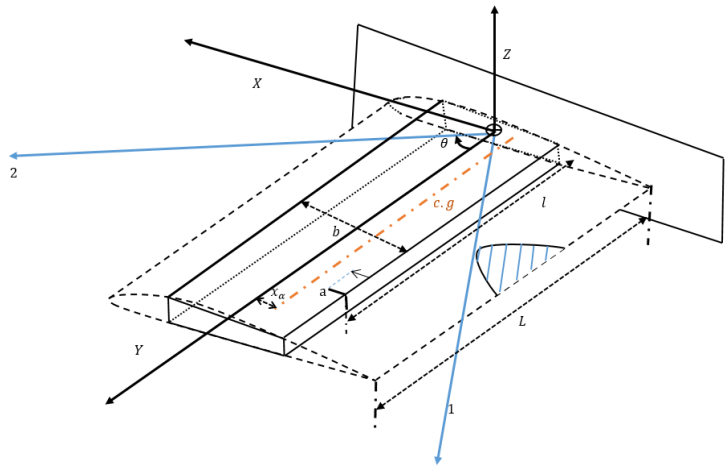

Fig. 1 coordinate system and notation for a bending-torsion coupled composite wing

Where $\mathrm{h}(y,t)$ is the bending displacement of a point on the elastic axis and $\psi(y,t)$ is the torsional displacement about the elastic axis, EI and GJ are the bending and torsional stiffness's, respectively. Mass moment of inertia about the elastic axis is denoted by I_α and x_α is the distance between the inertia axis and the elastic axis. Assuming harmonic oscillation for bending and torsion motions

$$\mathrm{h}(y,t) = \mathrm{H}(y)e^{i\omega t}, \psi(y,t) = \Psi(y)e^{i\omega t} \tag{2}$$

With substituting Eq. (2) in Eq. (1) and definition of a dimensionless variable($\xi = y/L$)

$$\begin{aligned} \frac{EI}{L^4}\frac{\partial^4 \mathrm{H}}{\partial \xi^4} - m\omega^2 \mathrm{H} &= \frac{K}{L^3}\frac{\partial^3 \psi}{d\xi^3} + mx_\alpha\omega^2\psi, \\ \frac{K}{L^3}\frac{\partial^3 \mathrm{H}}{\partial \xi^3} - mx_\alpha\omega^2 \mathrm{H} &= \frac{GJ}{L^2}\frac{d^2\psi}{d\xi^2} + I_\alpha\omega^2\psi \end{aligned} \tag{3}$$

Derived expressions regarding dimensionless variable are

$$\begin{aligned} \frac{\partial \mathrm{H}}{\partial y} = \frac{1}{L}\frac{\partial \mathrm{H}}{\partial \xi}, \frac{\partial^2 \mathrm{H}}{\partial y^2} = \frac{1}{L^2}\frac{\partial^2 \mathrm{H}}{\partial \xi^2}, \dots, \\ \frac{\partial^4 \mathrm{H}}{\partial y^4} = \frac{1}{L^4}\frac{\partial^4 \mathrm{H}}{\partial \xi^4}, \frac{\partial^3 \psi}{\partial y^3} = \frac{1}{L^3}\frac{\partial^3 \psi}{\partial \xi^3} \end{aligned} \tag{4}$$

By defining a differential operator $D = d(.)/d\xi$ and rearranging

$$\begin{aligned} \left(\frac{K}{L^3}D^3 - mx_\alpha\omega^2\right)\left(\frac{K}{L^3}D^3 + mx_\alpha\omega^2\right) \\ = \left(\frac{GJ}{L^2}D^2 + I_\alpha\omega^2\right)\left(\frac{EI}{L^4}D^4 - m\omega^2\right) \end{aligned} \tag{5}$$

Eventually, a sixth order ordinary differential equation is obtained as

$$\begin{aligned} \left(\frac{EI.GJ}{L^6} - \frac{K^2}{L^6}\right)D^6 + I_\alpha\omega^2\frac{EI}{L^4}D^4 - m\omega^2\frac{GJ}{L^2}D^2 - mI_\alpha\omega^2 \\ + m^2{x_\alpha}^2\omega^4 = 0 \end{aligned} \tag{6}$$

Rearranging leads to auxiliary equation as

$$\left(D^6 + \hat{a}D^4 - \hat{b}D^2 - \hat{a}\hat{b}\hat{c}\right)\mathrm{W} = 0, \mathrm{W} = \mathrm{H} \ or \ \Psi \tag{7}$$

where $\hat{a}$, $\hat{b}$ and $\hat{c}$ are defined in Appendix B. General solution for a differential equation of six order consists of one pair of real root $(\alpha, -\alpha)$ and two pair of pure imaginary roots $\left((i\beta, -i\beta), (i\gamma, -i\gamma)\right)$ as

$$\begin{aligned} \frac{\partial^6 \mathrm{W}}{\partial \xi^6} + \hat{a}\frac{\partial^4 \mathrm{W}}{\partial \xi^4} - \hat{b}\frac{\partial^2 \mathrm{W}}{\partial \xi^2} - \hat{a}\hat{b}\hat{c}\mathrm{W} = 0 \\ \mathrm{W}(\xi) = C_1\, cosh\, \alpha\xi + C_2\, sinh\, \alpha\xi + C_3\, cos\, \beta\xi + \\ C_4\, sin\, \beta\xi + C_5\, cos\, \gamma\xi + C_6\, sin\, \gamma\xi \end{aligned} \tag{8}$$

In which $C_1 - C_6$ are constants and parameters $\alpha, \beta \ and \ \gamma$ will be defined in appendix C. Thus mode shapes related to bending and torsion modes will be as

$$\begin{Bmatrix} \mathrm{H}(\xi) \\ \Psi(\xi) \end{Bmatrix} = \begin{bmatrix} A_1 & A_2 & A_3 & A_4 & A_5 & A_6 \\ B_1 & B_2 & B_3 & B_4 & B_5 & B_6 \end{bmatrix} \begin{Bmatrix} cosh\, \alpha\xi \\ sinh\, \alpha\xi \\ cos\, \beta\xi \\ sin\, \beta\xi \\ cos\, \gamma\xi \\ sin\, \gamma\xi \end{Bmatrix} \tag{9}$$

$A_1 - A_6$and $B_1 - B_6$ are two different sets of constants. By substituting general solutions in the Eq. (1), A and B coefficients are

$$\begin{aligned} B_1 = -\frac{e_\alpha g_\alpha}{L}A_1 + \frac{e_\alpha}{L}A_2, B_2 = \frac{e_\alpha}{L}A_1 - \frac{e_\alpha g_\alpha}{L}A_2, \\ B_3 = \frac{e_\beta g_\beta}{L}A_3 + \frac{e_\beta}{L}A_4, B_4 = -\frac{e_\beta}{L}A_3 + \frac{e_\beta g_\beta}{L}A_4, \\ B_5 = \frac{e_\gamma g_\gamma}{L}A_5 + \frac{e_\gamma}{L}A_6, B_6 = -\frac{e_\gamma}{L}A_5 + \frac{e_\gamma g_\gamma}{L}A_6. \end{aligned} \tag{10}$$

For more details refer to Appendix F. According to (Banerjee *et al*. 2008)

$$e_\alpha = \frac{k_\alpha}{1-g_\alpha^2}, g_\alpha = \frac{\bar{b}k_\delta}{\alpha^3}, k_\alpha = \frac{EI}{K}\frac{\bar{b}-\alpha^4}{\alpha^3},$$
$$e_\beta = \frac{k_\beta}{1+g_\beta^2}, g_\beta = \frac{\bar{b}k_\delta}{\beta^3}, k_\beta = \frac{EI}{K}\frac{\bar{b}-\beta^4}{\beta^3}, \quad (11)$$
$$e_\gamma = \frac{k_\gamma}{1+g_\gamma^2}, g_\gamma = \frac{\bar{b}k_\delta}{\gamma^3}, k_\gamma = \frac{EI}{K}\frac{\bar{b}-\gamma^4}{\gamma^3}$$

which

$$k_\delta = \frac{x_\alpha EI}{LK}, \bar{b} = \frac{m\omega^2 L^4}{EI} \quad (12)$$

Thus Eq. (9) will be converted to

$$\mathrm{H}(\xi) = \boldsymbol{A}\times\boldsymbol{\Gamma}, \Psi(\xi) = \boldsymbol{B}\times\boldsymbol{\Gamma}, \boldsymbol{B} = \boldsymbol{A}\times\boldsymbol{P} \quad (13)$$

$$\begin{cases}\boldsymbol{A} = [A_1 \quad A_2 \quad A_3 \quad A_4 \quad A_5 \quad A_6] \\ \boldsymbol{B} = [B_1 \quad B_2 \quad B_3 \quad B_4 \quad B_5 \quad B_6]\end{cases}, \boldsymbol{\Gamma} = \{cosh\alpha\xi, sinh\alpha\xi, cos\beta\xi, sin\,\beta\xi, cos\,\gamma\xi, sin\,\gamma\xi\}^T \quad (14)$$

$$\boldsymbol{P} = \begin{bmatrix} -\frac{e_\alpha g_\alpha}{L} & \frac{e_\alpha}{L} & 0 & 0 & 0 & 0 \\ \frac{e_\alpha}{L} & -\frac{e_\alpha g_\alpha}{L} & 0 & 0 & 0 & 0 \\ 0 & 0 & \frac{e_\beta g_\beta}{L} & -\frac{e_\beta}{L} & 0 & 0 \\ 0 & 0 & \frac{e_\beta}{L} & \frac{e_\beta g_\beta}{L} & 0 & 0 \\ 0 & 0 & 0 & 0 & \frac{e_\gamma g_\gamma}{L} & \frac{e_\gamma}{L} \\ 0 & 0 & 0 & 0 & -\frac{e_\gamma}{L} & \frac{e_\gamma g_\gamma}{L} \end{bmatrix} \quad (15)$$

3. Free vibration analysis of an intact beam

According to the normalized form of the general solution, there are six unknown coefficients as $\boldsymbol{A}$ and $\boldsymbol{B}$ coefficients are dependent together. Thus, to determine these coefficients a set of six equations are required. For a cantilevered beam theses equations are

-At the fixed end, $\xi = 0$

$$\mathrm{H}(0) = \Theta(0) = \Psi(0) = 0 \quad (16)$$

-At the free end, $\xi = 1$

$$\mathrm{M}(1) = \mathrm{S}(1) = \mathrm{T}(1) = 0 \quad (17)$$

The cross-sectional rotation $\Theta(\xi)$, the bending moment $\mathrm{M}(\xi)$, the shear force $\mathrm{S}(\xi)$, and the torsional moment $\mathrm{T}(\xi)$ at any cross section with the normalized coordinate ξ are (Banerjee *et al.* 2008)

$$\Theta(\xi) = \frac{1}{L}\frac{d\mathrm{H}(\xi)}{d\xi} = \Theta_1 A_1 + \Theta_2 A_2 + \Theta_3 A_3 + \Theta_4 A_4 + \Theta_5 A_5 + \Theta_6 A_6 \quad (18)$$

$$\mathrm{S}(\xi) = \frac{EI}{L}\frac{d^3\mathrm{H}(\xi)}{d\xi^3} + \frac{K}{L^2}\frac{d^2\Psi(\xi)}{d\xi^2} = S_1 A_1 + S_2 A_2 + S_3 A_3 + S_4 A_4 + S_5 A_5 + S_6 A_6 \quad (19)$$

$$\mathrm{M}(\xi) = -\frac{EI}{L^2}\frac{d^2\mathrm{H}(\xi)}{d\xi^2} - \frac{K}{L}\frac{d\Psi(\xi)}{d\xi} = M_1 A_1 + M_2 A_2 + M_3 A_3 + M_4 A_4 + M_5 A_5 + M_6 A_6 \quad (20)$$

$$\mathrm{T}(\xi) = -\frac{K}{L^2}\frac{d^2\mathrm{H}(\xi)}{d\xi^2} - \frac{GJ}{L}\frac{d\Psi(\xi)}{d\xi} = T_1 A_1 + T_2 A_2 + T_3 A_3 + T_4 A_4 + T_5 A_5 + T_6 A_6 \quad (21)$$

Coefficients in Eqs. (18)-(21) are defined in Appendix D. Applying six boundary conditions from Eqs. (16) and (17) and Eqs. (18)-(21) leads to

$$\mathrm{H}(0) = 0 \rightarrow \mathrm{H}(\xi = 0) = A_1 + A_3 + A_5 = 0 \quad (22)$$

$$\Psi(0) = 0 \rightarrow \Psi(\xi = 0) = B_1 + B_3 + B_5 = 0 \rightarrow \left(-\frac{e_\alpha g_\alpha}{L}A_1 + \frac{e_\alpha}{L}A_2\right) + \left(\frac{e_\beta g_\beta}{L}A_3 + \frac{e_\beta}{L}A_4\right) + \left(\frac{e_\gamma g_\gamma}{L}A_5 + \frac{e_\gamma}{L}A_6\right) = 0 \quad (23)$$

$$\Theta(0) = 0 \rightarrow \Theta(\xi = 0) = \frac{1}{L}\frac{d\mathrm{H}(\xi = 0)}{d\xi} = \frac{1}{L}(A_2\alpha + A_4\beta + A_6\gamma) = 0 \quad (24)$$

$$\mathrm{M}(\xi) = -\frac{EI}{L^2}\frac{d^2\mathrm{H}(\xi)}{d\xi^2} - \frac{K}{L}\frac{d\Psi(\xi)}{d\xi} \xrightarrow{\mathrm{M}(\xi=1)=0}$$
$$\mathrm{M}(\xi) = M_1(1)A_1 + M_2(1)A_2 + M_3(1)A_3 + M_4(1)A_4 + M_5(1)A_5 + M_6(1)A_6 = 0 \quad (25)$$

$$\mathrm{S}(\xi) = \frac{EI}{L^3}\frac{d^3\mathrm{H}(\xi)}{d\xi^3} + \frac{K}{L^2}\frac{d^2\Psi(\xi)}{d\xi^2} \xrightarrow{\mathrm{S}(\xi=1)=0}$$
$$\mathrm{S}(\xi) = S_1(1)A_1 + S_2(1)A_2 + S_3(1)A_3 + S_4(1)A_4 + S_5(1)A_5 + S_6(1)A_6 = 0 \quad (26)$$

$$\mathrm{T}(\xi) = -\frac{K}{L^2}\frac{d^2\mathrm{H}(\xi)}{d\xi^2} - \frac{GJ}{L}\frac{d\Psi(\xi)}{d\xi} \xrightarrow{\mathrm{T}(\xi=1)=0}$$
$$\mathrm{T}(\xi) = T_1(1)A_1 + T_2(1)A_2 + T_3(1)A_3 + T_4(1)A_4 + T_5(1)A_5 + T_6(1)A_6 = 0 \quad (27)$$

From Eqs. (22)-(27) matrix equation is obtained as

$$\begin{bmatrix} a_{11} & a_{12} & a_{13} & a_{14} & a_{15} & a_{16} \\ a_{21} & a_{22} & a_{23} & a_{24} & a_{25} & a_{26} \\ a_{31} & a_{32} & a_{33} & a_{34} & a_{35} & a_{36} \\ a_{41} & a_{42} & a_{43} & a_{44} & a_{45} & a_{46} \\ a_{51} & a_{52} & a_{53} & a_{54} & a_{55} & a_{56} \\ a_{61} & a_{62} & a_{63} & a_{64} & a_{65} & a_{66} \end{bmatrix} \begin{bmatrix} A_1 \\ A_2 \\ A_3 \\ A_4 \\ A_5 \\ A_6 \end{bmatrix} = \begin{bmatrix} 0 \\ 0 \\ 0 \\ 0 \\ 0 \\ 0 \end{bmatrix} \rightarrow \boldsymbol{\Lambda}\times\boldsymbol{A}^T = 0 \quad (28)$$

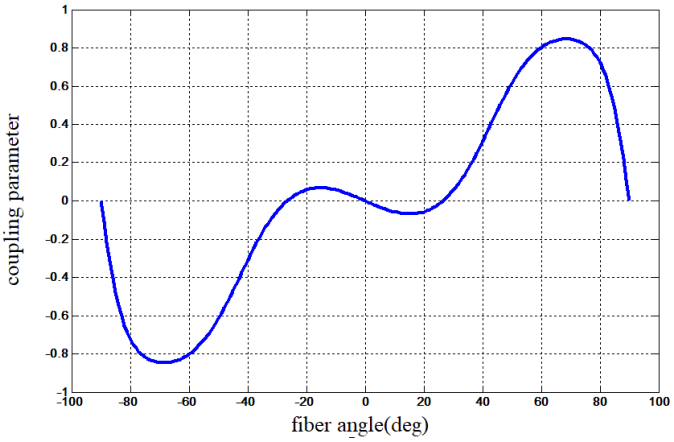

Fig. 2 Coupling parameter changes w.r.t fiber angle

Table 1 Properties of case study I (composite Goland wing)

Bending rigidity	$EI = 9.75 \times 10^6 \text{N.m}^2$
Torsional rigidity	$GJ = 9.88 \times 10^5 \text{N.m}^2$
Bending–Torsion coupling rigidity	$K = 0,1.5,2,2.5 \times 10^6 \text{N.m}^2$
Mass per unit length	$m = 35.75$ kg/m
Mass moment of inertia per unit length	$I_\alpha = 8.65$ kg.m
Distance between the mass and elastic axes	$x_\alpha = 0,0.1,0.2,0.3$ m
Length	L = 6 m
Width	b = 1.83 m

The natural frequencies are gained when the coefficients matrix determinant (dynamic stiffness matrix) is equal to zero ($|\boldsymbol{\Lambda}| = 0$).

3.1 Coupling parameter

According to the publication (Wang 2004), dimensionless coupling measure is defined as

$$\Pi = \frac{K}{\sqrt{EI.GJ}} \rightarrow \begin{cases} \Pi = 0 \rightarrow \text{no coupling,} \\ \Pi = \pm 1 \rightarrow \text{strongest coupling} \end{cases} \quad (29)$$

By plotting coupling parameter versus fiber angle in Fig. 2 it is obvious that no coupling case is related to fiber angles: 0, 30, 90deg and the strongest coupling case is related to fiber angle :70deg.

For conventional layup in composite wings such as $[0,90,\pm 45]_s$ and thickness of 0.005m for any ply, coupling parameter is equal to 0.1516, this value is near to coupling parameter for layup 35 deg. Thus, to simplifying the calculations a simple layup 35 deg can be used instead of aforementioned conventional layup as unidirectional composite wing.

4. Results and validation

In this paper three case studies were considered for intact wing. Case study I which is Goland composite wing or Banerjee study, case study II which is composite Minguet wing and case study III which is Wang composite wing. In all these cases validation results were provided and the comparison of the results were given in Table 2, Tables 4 and 6. For validation of cracked wing results, only Wang composite wing is selected and the comparison of the results were given in Table 7.

4.1 Intact beam results

In order to validate and confirm the outcome of the model approach in MATLAB and the accuracy of the theory, two illustrative examples are chosen from the works of Minguet (1989) and Banerjee *et al*. (2008) which were also used in previous literature then the model approach is developed to case study III.

4.1.1 Verification by the case study I: Goland wing

A cantilever composite wing whose stiffness and mass properties are similar to that of the metallic wing is used by Goland except for the bending–torsion coupling rigidity (K) which does not apply to a metallic wing. However, K is an important parameter for a composite wing. The basic data used for the wing are given in Table 1. Complete consistent between present study and reference study (Banerjee et al. 2008) is illustrated in Table 2.

4.1.2 Verification by the case study II: Minguet wing

The properties of case study II are given in Table 3. Also results and comparison with study Banerjee *et al.* (2008) is listed in Table 4.

Table 2 Results comparison between present study and study Banerjee *et al.* (2008) for intact beam

x_α(m)	K ($\times 10^6$N.m^2)	Natural frequencies (rad/s)					
		Present study			Banerjee et al. (2008)		
		f_1	f_2	f_3	f_1	f_2	f_3
0	0	51.05	88.45	265.25	51	88.47	265.44
	1.5	42.7	91.14	212.38	42.68	91.21	212.44
	2	36.30	91.58	181.60	36.28	91.65	181.63
	2.5	27.34	87.14	146.03	27.32	87.18	146.03
0.1	0	50.55	90.93	258.25	50.53	91.02	258.43
	1.5	40.26	98.99	197.52	40.25	99.07	197.57
	2	33.97	100.39	168.52	33.96	100.4	168.55
	2.5	25.46	94.78	137.33	25.44	94.81	137.34
0.2	0	49.34	99.10	246.48	49.33	99.20	246.60
	1.5	38.08	112.12	185.54	38.07	112.22	185.57
	2	31.99	114.61	157.80	31.98	114.71	157.81
	2.5	23.90	104.34	133.82	23.88	104.36	133.87
0.3	0	47.75	115.59	238	47.74	115.74	238.10
	1.5	36.15	134.70	177.11	36.14	134.86	177.15
	2	30.29	139.80	148.83	30.28	139.97	148.83
	2.5	22.59	109.65	146.88	22.57	109.62	147.03

Table 3 Properties of case study II (composite Minguet wing)

Bending rigidity	$EI = 0.0143$ N.m^2
Torsional rigidity	$GJ = 0.0195$ N.m^2
Bending–Torsion coupling rigidity	$K = 0.00632$ N.m^2
Mass per unit length	$m = 0.0238$ kg/m
Mass moment of inertia per unit length	$I_\alpha = 1.66 \times 10^{-6}$ kg.m
Distance between the mass and elastic axes	$x_\alpha = 0$
Length	L = 0.56 m
Width	b = 0.03 m
thickness	t=0.00054 m
layup	$[0^0, 45^0]_s$

Table 4 Results comparison between present study, and other studies for intact beam

Frequency number	Natural Frequency (rad/s)		
	Minguet 1989	Banerjee *et al.* (2008)	Present Study.
1	8.04	8.04	8.045
2	50.32	50.39	50.395
3	141.4	141	141.025
4	279	276	275.985
5	306	304.3	304.285

4.1.3 Verification by the case study III: Wang wing

The unidirectional composite beam consists of several plies aligned in the same direction. In each ply (and for the whole laminate) the material is assumed orthotropic regarding to corresponding axes of symmetry. Material and geometric properties of the beam are given in Table 5.

Table 5 Properties of case study III (Wang 2004)

Modulus of elasticity-matrix	E_m=2.76 × 10^9 N/m^2
Modulus of elasticity-fiber	E_f=275.6 × 10^9 N/m^2
Modulus of rigidity-matrix	G_m=1.036 × 10^9 N/m^2
Modulus of rigidity-fiber	G_f=114.8 × 10^9 N/m^2
Mass density of matrix	ρ_m=1600 kg/m^3
Mass density of fiber	ρ_f=1900 kg/m^3
Length	L = 0.5 m
Width	b = 0.1 m
Thickness	t=0.005 m
fiber angle	$\theta = 30^0, 70^0$
Offset of the center of gravity	x_α = 0

Table 6 Results comparison for intact beam in case study III (Wang 2004)

Intact beam	$\theta = 30^0$	f_1	f_2	f_3	f_4
	Wang 2004	42.35	265.42	554.38	743.41
	Present study	42.35	265.45	554.35	743.25
	$\theta = 70^0$	f_1	f_2	f_3	f_4
	Wang 2004	75.2	445.6	916.1	1179.7
	Present study	76.05	465.85	896.55	1220.3
	$\theta = 0^0$	f_1	f_2	f_3	f_4
	Wang 2004	43.6	273.1	413.5	764.7
	Present study	43.55	273.15	411.65	764.75
	$\theta = 90^0$	f_1	f_2	f_3	f_4
	Wang 2004	181	413.5	1134.5	1240.6
	Present study	181.05	411.65	1134.6	1235.1
	$\theta = 35^0$	f_1	f_2	f_3	f_4
	Present study	43.85	268.25	603.35	750.75

4.2 Free vibration analysis of the cracked beam

To model a cracked beam such as Wang and Inman (2007) a beam can be replaced with two intact beams connected in the crack location. Then, additional boundary conditions are defined in the crack location by local flexibility method and Castigliano's theorem. Replacing the cracked beam with two intact beams yields

$$\begin{cases} 0 \le \xi \le \xi_c \rightarrow \begin{cases} \mathrm{H}_1(\xi) = \boldsymbol{A} \times \boldsymbol{\Gamma}, \\ \Psi_1(\xi) = \boldsymbol{B} \times \boldsymbol{\Gamma}, \end{cases} \\ \xi_c \le \xi \le 1 \rightarrow \begin{cases} \mathrm{H}_2(\xi) = \widehat{\boldsymbol{A}} \times \boldsymbol{\Gamma}, \\ \Psi_2(\xi) = \widehat{\boldsymbol{B}} \times \boldsymbol{\Gamma} \end{cases} \end{cases} \tag{30}$$

$$\begin{cases} \widehat{\boldsymbol{A}} = [A_7 \quad A_8 \quad A_9 \quad A_{10} \quad A_{11} \quad A_{12}], \\ \widehat{\boldsymbol{B}} = [B_7 \quad B_8 \quad B_9 \quad B_{10} \quad B_{11} \quad B_{12}] \end{cases} \tag{31}$$

Which the relations between $\widehat{\boldsymbol{A}}$ and $\widehat{\boldsymbol{B}}$ coefficients, in the same approach for Eq.(10) are as

$$\begin{gathered} B_1 = -\frac{e_\alpha g_\alpha}{L} A_1 + \frac{e_\alpha}{L} A_2, B_2 = \frac{e_\alpha}{L} A_1 - \frac{e_\alpha g_\alpha}{L} A_2, \\ B_3 = \frac{e_\beta g_\beta}{L} A_3 + \frac{e_\beta}{L} A_4, B_4 = -\frac{e_\beta}{L} A_3 + \frac{e_\beta g_\beta}{L} A_4, \\ B_5 = \frac{e_\gamma g_\gamma}{L} A_5 + \frac{e_\gamma}{L} A_6, B_6 = -\frac{e_\gamma}{L} A_5 + \frac{e_\gamma g_\gamma}{L} A_6, \\ B_7 = -\frac{e_\alpha g_\alpha}{L} A_7 + \frac{e_\alpha}{L} A_8, B_8 = \frac{e_\alpha}{L} A_7 - \frac{e_\alpha g_\alpha}{L} A_8, \\ B_9 = \frac{e_\beta g_\beta}{L} A_9 + \frac{e_\beta}{L} A_{10}, B_{10} = -\frac{e_\beta}{L} A_9 + \frac{e_\beta g_\beta}{L} A_{10}, \\ B_{11} = \frac{e_\gamma g_\gamma}{L} A_{11} + \frac{e_\gamma}{L} A_{12}, \\ B_{12} = -\frac{e_\gamma}{L} A_{11} + \frac{e_\gamma g_\gamma}{L} A_{12} \end{gathered} \tag{32}$$

Similar to intact beam boundary conditions in fixed and free ends, the boundary conditions will be the same as Eqs. (16) and (17). The additional boundary conditions or continuity boundary conditions in crack location are

$$\begin{gathered} \mathrm{M}_1(\xi_c) = \mathrm{M}_2(\xi_c), \mathrm{S}_1(\xi_c) = \mathrm{S}_2(\xi_c), \mathrm{T}_1(\xi_c) = \mathrm{T}_2(\xi_c), \\ \mathrm{H}_2(\xi_c) = \mathrm{H}_1(\xi_c) + c_{22}\mathrm{S}_1(\xi_c) + c_{26}\mathrm{T}_1(\xi_c), \\ \Theta_2(\xi_c) = \Theta_1(\xi_c) + c_{44}\mathrm{M}_1(\xi_c), \end{gathered} \tag{33}$$

Table 7 Results comparison for cracked beam in case study I

	$\theta = 30^0$	f_1	f_2	f_3	f_4
Cracked beam Crack length:0.3 Crack location:0.3	Wang 2004	39.03	259.77	531.15	683.31
	Present study	41.85	242.35	546.05	709.35
	$\theta = 70^0$	f_1	f_2	f_3	f_4
	Wang 2004	67.95	441.88	665.15	1144.8
	Present study	69.85	304.85	903.05	1084.1
	$\theta = 35^0$	f_1	f_2	f_3	f_4
	Present study	42.35	245.05	595.25	716.75
	$\theta = 90^0$	f_1	f_2	f_3	f_4
	Present study	170.65	409.75	800.45	1212.8
	$\theta = 0^0$	f_1	f_2	f_3	f_4
	Present study	42.95	243.45	409.75	722.45

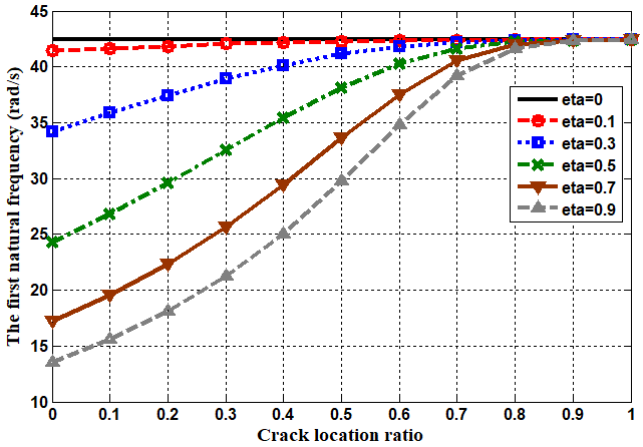

Fig. 3 The first natural frequency changes w.r.t crack locations in various crack depth ratio (eta) for case study I at fiber angle 30 deg

$$\Psi_2(\xi_c) = \Psi_1(\xi_c) + c_{62}\mathrm{S}_1(\xi_c) + c_{66}\mathrm{T}_1(\xi_c)$$

c_{ij} are coefficients of local flexibility matrix $\boldsymbol{C}$ which these are defined in Appendix E.

$$\boldsymbol{C} = \begin{bmatrix} c_{22} & 0 & c_{26} \\ 0 & c_{44} & 0 \\ c_{62} & 0 & c_{66} \end{bmatrix} \tag{34}$$

According to the general solution in the normalized form, the number of unknown coefficients is equal to twelve, because $\boldsymbol{B}$, $\boldsymbol{A}$ and $\widehat{\boldsymbol{B}}$, $\widehat{\boldsymbol{A}}$ coefficients are related. Thus, to find the coefficients twelve equations are required.

From the paper (Wang 2004), the cross-sectional rotation $\Theta(\xi)$, the bending moment $\mathrm{M}(\xi)$, the shear force $\mathrm{S}(\xi)$ and the torsional moment $\mathrm{T}(\xi)$ at any cross section with the normalized coordinate ξ will be similar to Eqs.(18)-(21) From Eqs. (16) and (17) and Eq. (33) related to boundary conditions, matrix becomes

$$[\boldsymbol{\Lambda}]_{12\times12}[\boldsymbol{\mathcal{A}}^{\boldsymbol{T}}]_{12\times1} = [0]_{12\times1}, \boldsymbol{\mathcal{A}} = [\boldsymbol{A}:\widehat{\boldsymbol{A}}] \tag{35}$$

Again, the natural frequencies are equal to frequencies that lead to zeroing coefficients matrix (dynamic stiffness matrix) determinant ($|\boldsymbol{\Lambda}| = 0$). In order to determine the crack effects on vibration analysis, three case studies are investigated and natural frequencies and shape functions are extracted and compared with previous works.

4.2.1 Verification by the case study I: Wang wing

According to cracked wing model (Wang 2004) and properties in Table 5 and applying dynamic stiffness matrix approach (Banerjee *et al*. 2008), as it is given in Tables 6 and 7, in fiber angles 30 and 70 deg, natural frequency for intact beam is equal to 42.35 rad/sec and for cracked wing the natural frequency is 39.03 rad/sec while according to present study the natural frequency for cracked beam is 38.95 rad/sec. This conclusion is extensional for other fiber angles.

From this analysis, the following results are obtained:

1- Mode shapes of cracked wing in Wang's model shows that in crack location there is a discontinuity and the most discontinuity happens in torsion mode which is the fiber angle of 70 deg. Therefore,

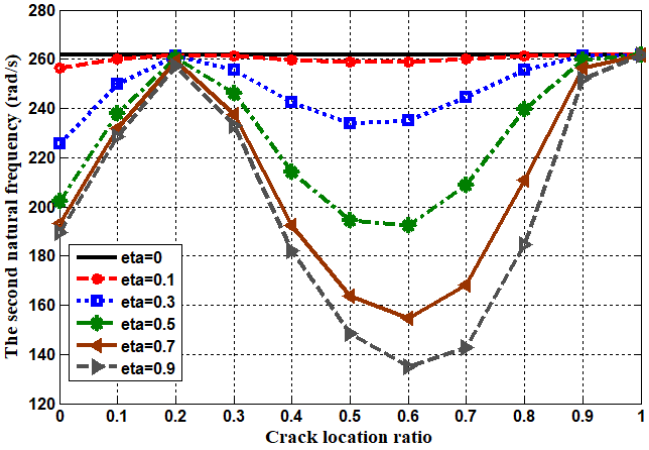

Fig. 4 The second natural frequency changes w.r.t crack locations in various crack depth ratio (eta) for case study I at fiber angle 30 deg

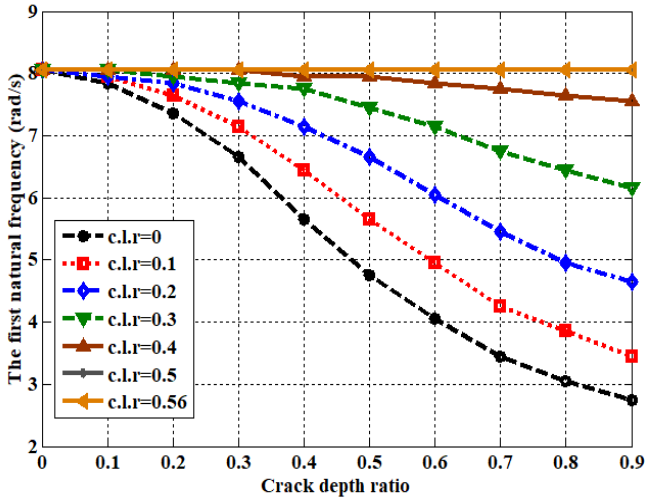

Fig. 5 The first natural frequency changes w.r.t crack depths in various crack location ratios (c.l.r) for case study II

at this fiber angle this mode can be used as a base for mode shapes of cracked wing in aero-elastic analysis.

2- The first natural frequency changes with respect to fiber angles (at dimensionless crack location of 0.3 and dimensionless crack depth of 0.3) shows that by increasing the fiber angle, the first natural frequency is increased and the highest first natural frequency is located at the fiber angle of 85 deg.

3- The first natural frequency variations with respect to crack location ratio (at the fiber angle 30deg and dimensionless crack depth 0.3) shown that the lowest of the first natural frequency has happened when the crack location is at the root and the highest frequency has happened when the crack location is at tip. Thus, whatever the crack's location farther away from wing root, the first natural frequency is higher and the wing structure is better (Figs. 3 and 4).

4- The first natural frequency changes with respect to crack depth ratio (at fiber angle 30deg and various crack location ratio) shows that by increasing the crack depth ratio (eta), the first natural frequency is decreased and this behaviour is more intensive for the crack location at the root.

5- Due to coupling terms, in non- coupling case (30deg) there are good agreements between present study results and the Wang's paper (Wang 2004). But in strongest coupling case (70deg) there are weak agreements.

4.2.2 Case study II: Minguet wing

The second illustrative example of bending-torsion coupled composite beams available in the literature is the flat composite beam of four ply carbon-fiber reinforced plastic material (Minguet 1989) with lay-up [45deg/0deg], length 0.56 m, width 0.03m and thickness 0.00054 m. The rigidities and other properties are given in Table 3. Fig. 5 to Fig. 8 illustrates changes of the first natural frequency of wing with crack location and crack depth variations.

As illustrated in Figs. 5 and 6, maximum decreasing of the first natural frequency is related to crack location at the root, and maximum decreasing of the second natural frequency is related to crack location ratio 0.3.

Fig. 7 similar to Fig. 3 shows an increasing trend for the natural frequency when the edge crack approaches to the tip

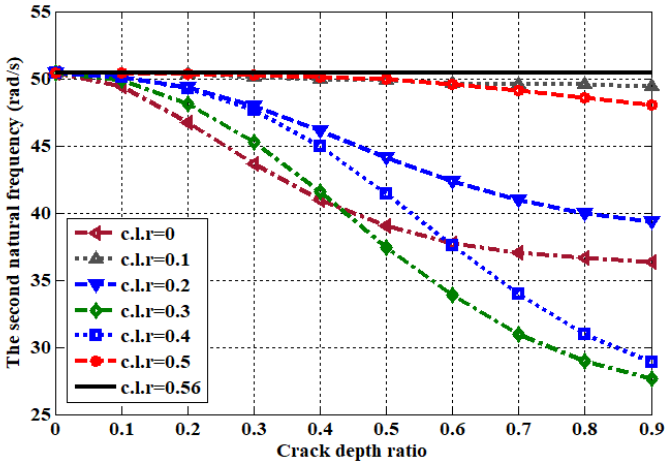

Fig. 6 The second natural frequency changes w.r.t crack depths in various crack location ratios (c.l.r) for case study II

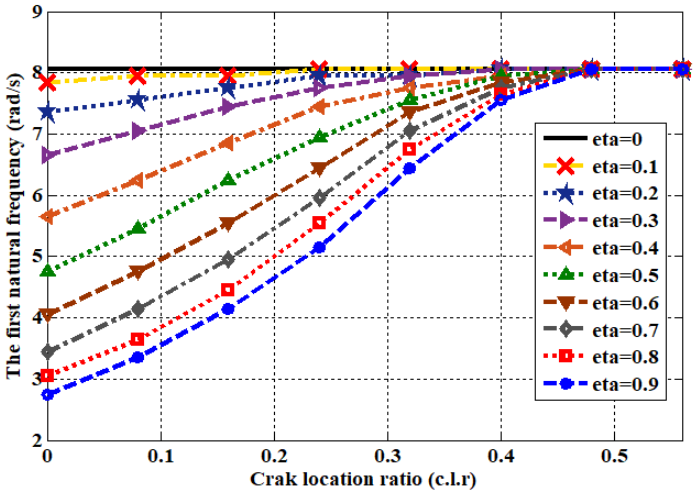

Fig. 7 The first natural frequency changes w.r.t crack locations in various crack depths (eta) for case study II

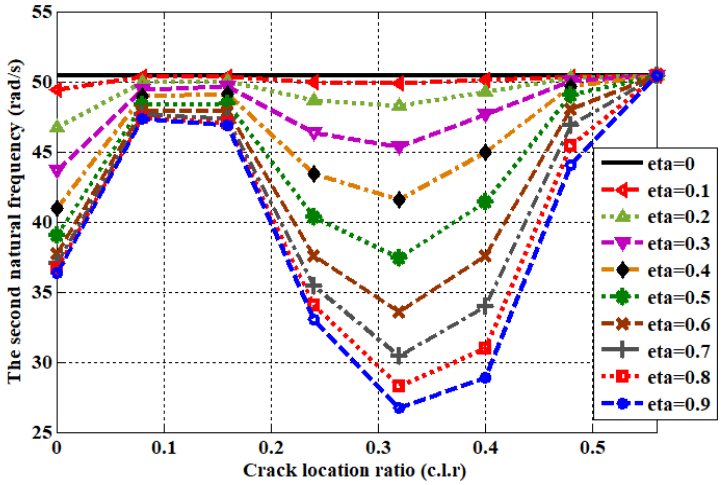

Fig. 8 The second natural frequency changes w.r.t crack locations in various crack depths (eta) for case study II

of the wing. Of course this trend is different for the second natural frequency. Regarding Fig. 8 (similar to Fig. 4), for crack location ratio between 0 to 0.08 the trend is increasing, between 0.08 to 0.16 trend is almost constant,

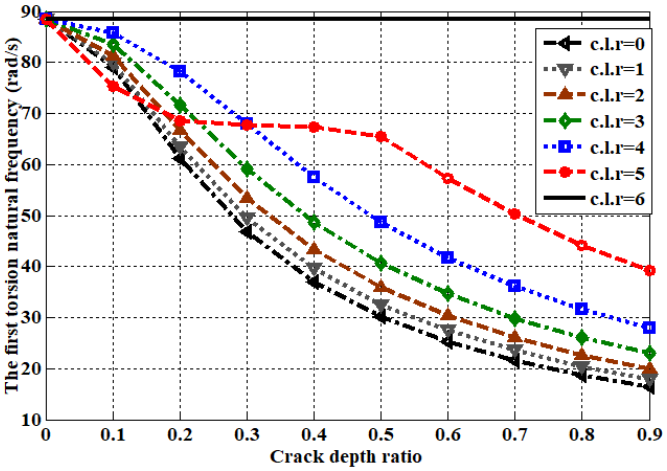

Fig. 9 Natural frequency changes w.r.t crack depths in various crack location ratios (c.l.r) for Goland wing in torsion mode

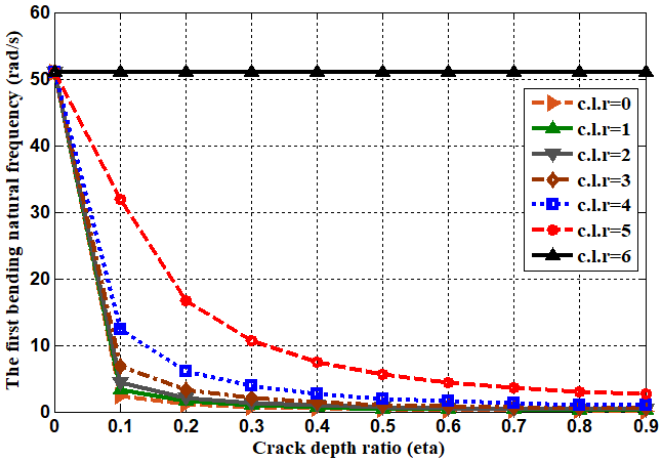

Fig. 10 Natural frequency changes w.r.t crack depths in various crack location ratios (c.l.r) for Goland wing in bending mode

Table 8 simple verification of developed code for Goland wing

Crack depth	0
Crack location	0
Fiber angle	0
Bending–torsion coupling rigidity (K)	10e-6
Geometric coupling parameter ($\boldsymbol{x_\alpha}$)	0
Bending natural frequency (rad/s)	51.05
Torsion natural frequency (rad/s)	88.45

between 0.16 to 0.32 it is decreasing and between 0.32 to 0.56 the trend is again increasing.

4.2.3 Case study III: Goland wing

As it was seen in previous section, the edge crack obviously reduced the first natural frequency of the cracked beam. In this subsection, the edge crack effects on high aspect ratio composite Goland wing with properties given in Table 1 will be investigated. The Goland wing model used in this work is based on the described model by Banerjee *et al.* (2008). The model (Fig. 1) represents a cantilevered wing with a 6 m span and 1.83 m chord.

To verify the model approach, the crack depth was set to zero as an input and after finding the natural frequencies, the intact beam natural frequencies were obtained (Table 8).

Fig. 9 to Fig. 12 shows changes of the first natural frequency of Goland wing with crack location and crack depth variations at fiber angle 0deg, material coupling parameter 1e-6, distance between the mass and elastic axes 0 (geometric coupling parameter) for bending and torsion, respectively. In bending mode, by increasing the crack depth the bending natural frequency is reduced and it is more intensive where the downward trend of the crack location approaches to the root. In addition, in torsion mode the same trend happens with lower slope.

In Figs. 11 and 12, upward behaviour of the first natural frequency in bending and torsion modes has been plotted for crack location from the root to the tip. It is showed that the first natural frequency is increased by moving the crack from the root to the tip.

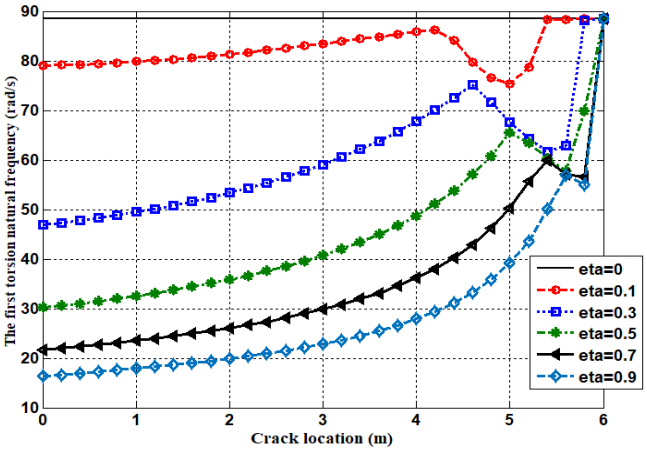

Fig. 11 The torsional natural frequency changes w.r.t crack locations in various crack depths (eta) for Goland wing

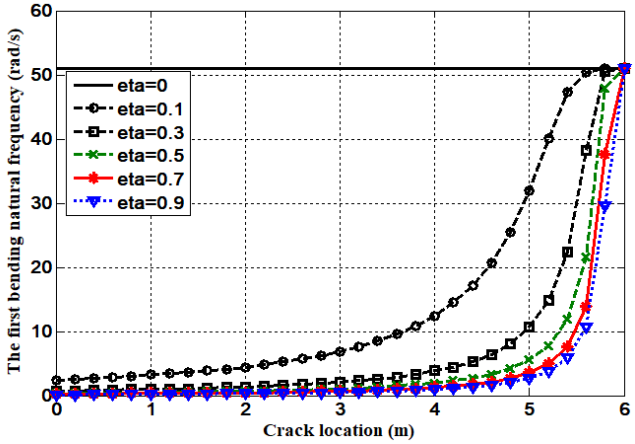

Fig. 12 The bending natural frequency changes w.r.t crack locations in various crack depths (eta) for Goland wing

Table 9 Natural frequencies for composite Goland wing

Crack depth	0.1	Natural frequencies (rad/s)	5.85
Crack location	3		82.05
Bending–torsion coupling rigidity (K)	1.5e6		115.85
Fiber angle (deg)	45		231.75
Geometric coupling parameter (x_α)	0.1		367.55
			486.65

To plot shape modes, assuming crack depth 0.1 m and crack location 3 m, the natural frequencies are derived as Table 9.

In Fig.13 to Fig.15 the first six mode shapes of composite Goland wing has been illustrated. It is obvious that there is a discontinuity in the crack location.

In Table 10 natural frequency changes regarding bending–torsion coupling rigidity (K) has been tabulated assuming crack depth 0.1m and crack location 3 m. In Fig. 16 the natural frequency changes regarding coupling parameter (K) has been illustrated in crack depth 0.1 m and crack location 3 m for different geometric coupling parameters. It is clear that in a certain coupling parameter, the highest of the first natural frequency has occurred at the highest of the geometric coupling parameter.

Finally the following results are obtained:

- Critical case study is related to case study III since most natural frequency reductions have occurred in this case.
- As illustrated in Table 11 critical crack location in the first natural frequency is related to the root of the wing but it is different in the second natural frequency depending on fiber angle and geometric and material couplings.

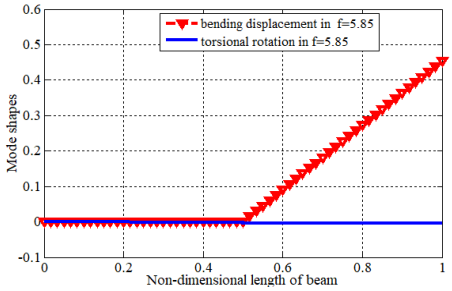

(a) Natural frequency 5.85 Hz

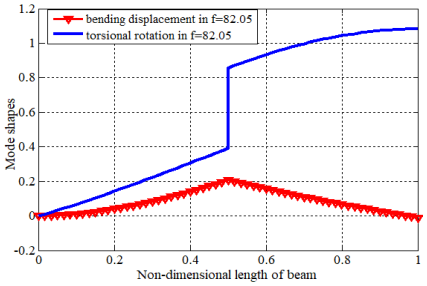

(b) Natural frequency 82.05 Hz

Fig.13 Mode shapes for composite Goland wing

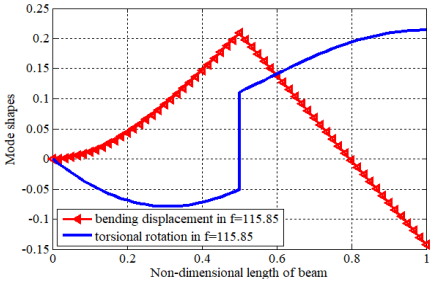

(a) Natural frequency 115.85 Hz

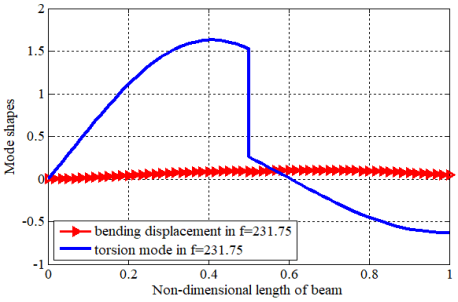

(b) Natural frequency 231.75 Hz

Fig.14 Mode shapes for composite Goland wing

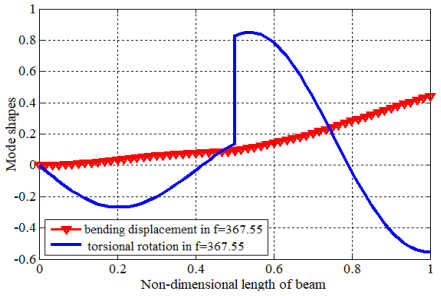

(a) Natural frequency 367.55 Hz

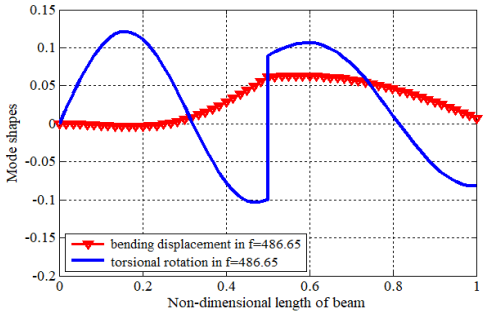

(b) Natural frequency 486.65 Hz

Fig. 15 Mode shapes for composite Goland wing

Table 10 Natural frequency changes w.r.t bending–torsion coupling rigidity in composite Goland wing

Crack depth:0.1, Crack location:3, Geometric coupling parameter (x_α):0.1		
Fiber angle	Bending–torsion coupling rigidity (K)	Natural frequencies (rad/s)
0	10e-6	6.85-66.95
35	0.5e6	6.85-68.35
40	1e6	6.55-72.75
45	1.5e6	5.85-82.05
52	2e6	4.85-250.55
60	2.5e6	3.45-242.85
70	2.63e6	3.05-221.95

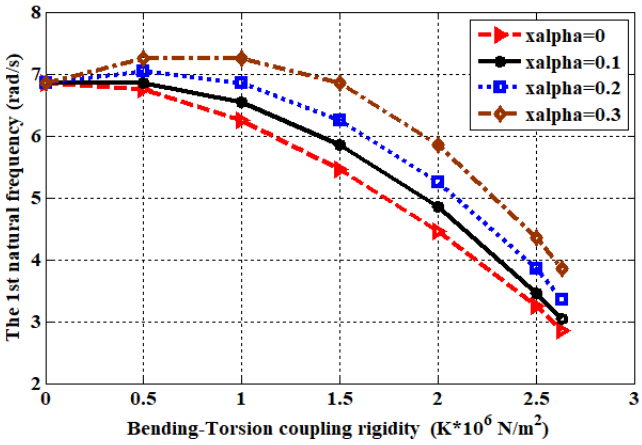

Fig. 16 Natural frequency changes w.r.t bending–torsion coupling rigidity (K), in crack depth: 0.1m and crack location:3 m for a range of values for geometric coupling parameter (x_α)

Table 11 Event conditions of the lowest natural frequency in case studies

	The first natural frequency			The second natural frequency		
	C.S* I	C.S II	C.S III	C.S I	C.S II	C.S III
eta	0.9×C**	0.9×C	0.9×C	0.9×C	0.9×C	0.9×C
ξ	root	root	root	0.6×S***	0.3×S	root

*Case Study, **Chord, ***Span

6. Conclusions

In this study the edge crack effects on modal properties of a composite wing is investigated. First, free vibration analysis of an intact wing, which modelled as an Euler-Bernouli cantilevered composite beam, is performed then the edge crack effects on modal properties are studied. Results showed that the edge crack reduced natural frequencies in both uncoupled case (30 deg) and strongest coupling case (70 deg). It also showed that the edge crack changes the mode shapes and the changes appeared as a breakage in crack location. These changes in strongest coupling case and torsional mode are more tangible than other cases. The first natural frequency corresponding to crack location showed that moving from wing root to wing tip increases the natural frequency. Also, increasing the crack depth decreases the natural frequency which is intensive in the wing root. The changes of first natural frequency w.r.t fiber angle showed that increasing the fiber angle decreases the first natural frequency for fiber angle less than 30 deg and increasing fiber angle increases the first natural frequency for fiber angle more than 30 deg. The highest first natural frequency has occurred in the fiber angle of 88 deg. The bending-torsion coupling rigidity showed that in fiber angle 0 and 90 deg there is no material coupling and the weakest coupling is in 30 deg and the strongest coupling is in 70 deg. Also the crack leads to a geometric coupling. At final mode-shapes of the cracked beam, the fiber angle of 70 deg could be selected as an input for aero-elastic analysis because the crack effect is the highest at this fiber angle. In the case studies three models for verification have been selected for an intact wing. Also for a cracked beam, three models have been selected including models of the intact beam. In this study, dynamic stiffness matrix formulation for coupled bending-torsion vibration of composite cracked beams is developed and the results is determined for a well-known cantilevered beam. The results showed that the crack (even with shallow depth) in root of large span wing severely decreases the natural frequency. Therefore structural designers should use from different methods such as aero-elastic tailoring and SHM to reduce this danger.

References

Ashour, A.S. (2003), "Buckling and vibration of symmetric laminated composite plates with edges elastically restrained", *Steel Compos. Struct.*, **3**(6), 439-450. https://doi.org/10.12989/scs.2003.3.6.439.

Banerjee, J.R. (2001), "Explicit analytical expressions for frequency equation and mode shapes of composite beams", *Int. J. Solids. Struct.*, **38**(14), 2415-2426. https://doi.org/10.1016/S0020-7683(00)00100-1.

Banerjee, J.R. and Su, H. (2006), "Dynamic stiffness formulation and free vibration analysis of a spinning composite beam", *Comput. Struct.*, **84**(19), 1208-1214. https://doi.org/10.1016/j.compstruc.2006.01.023.

Banerjee, J.R. and Williams, F.W. (1995), "Free Vibration of composite beams—an exact method using symbolic computation", *J. Aircraft*, **32**(3), 636-642. https://doi.org/10.2514/3.46767.

Banerjee, J.R., Su, H. and Jayatunga, C. (2008), "A dynamic stiffness element for free vibration analysis of composite beams

and its application to aircraft wings", *Comput. Struct.*, **86**(6), 573-579. https://doi.org/10.1016/j.compstruc.2007.04.027.

Boscolo, M. and Banerjee, J.R. (2012), "Dynamic stiffness formulation for composite Mindlin plates for exact modal analysis of structures. Part I: Theory", *Comput. Struct.*, **96**(97), 61-73. https://doi.org/10.1016/j.compstruc.2012.01.002.

Boscolo, M. and Banerjee, J.R. (2012), "Dynamic stiffness formulation for composite Mindlin plates for exact modal analysis of structures. Part II: Results and applications", *Comput. Struct*., **96**(97), 74-83. https://doi.org/10.1016/j.compstruc.2012.01.003.

Chronopoulos, D., Troclet, B., Bareille, O. and Ichchou, M. (2013). "Modeling the response of composite panels by a dynamic stiffness approach". *Compos. Struct*., 96, 111-120. https://doi.org/10.1016/j.compstruct.2012.08.047.

Daneshmehr, A., Nateghi, A. and Inman, D.J. (2013), "Free vibration analysis of cracked composite beams subjected to coupled bending-torsion loads based on a first order shear deformation theory", *Appl. Math. Model.*, **37**(24), 10074-10091. https://doi.org/10.1016/j.apm.2013.05.062.

Demir, E. (2016), "A study on natural frequencies and damping ratios of composite beams with holes", *Steel Compos. Struct.*, **21**(6), 1211-1226. https://doi.org/10.12989/scs.2016.21.6.1211.

Erdelyi, N.H. and Hashemi, S.M. (2016), "On the finite element free vibration analysis of delaminated layered beams: a new assembly technique", *J. Shock. Vib.*, **2016**, 1-14. http://dx.doi.org/10.1155/2016/3707658.

Hodges, D.H., Atilgan, A.R., Fulton, M.V. and Rehfied, L.W. (1991), "Free-vibration analysis of composite beams", *J. Am. Helicopter Soc.*, **36**(3), 36-47. https://doi.org/10.4050/JAHS.36.36.

Jafari-Talookolaei, R. A. (2015), "Analytical solution for the free vibration characteristics of the rotating composite beams with a delamination", *Aerosp. Sci. Technol.*, **45**, 346-358. https://doi.org/10.1016/j.ast.2015.06.009.

Kashani, M.T. and Hashemi, S.M. (2018), "A finite element formulation for bending-torsion coupled vibration analysis of delaminated beams under combined axial load and end moment", *J. Shock. Vib.*, **2018**, 1–12. https://doi.org/10.1155/2018/1348970.

Kim, N.I. (2009), "Dynamic stiffness matrix of composite box beams", *Steel Compos. Struct*., **9**(5), 473-497. https://doi.org/10.12989/scs.2009.9.5.473.

Krawczuk, M. and Ostachowicz, W.M. (1995), "Modelling and vibration analysis of a cantilever composite beam with a transverse open crack", *J. Sound Vib.*, **138**(1), 69-89. https://doi.org/10.1006/jsvi.1995.0239.

Lee, J. (2000), "Free vibration analysis of delaminated composite beams", *Comput. Struct.*, **74**(2), 121-129. https://doi.org/10.1016/S0045-7949(99)00029-2.

Ling, Z., Chen,J., Yinong, Y. and Ziqiang, L. (2015), "Flutter influence mode analysis of high speed wing model", *Procedia Eng*., **99**, 33-38. https://doi.org/10.1016/j.proeng.2014.12.504.

Liu, Y. and Shu, D.W. (2014), "Coupled bending-torsion vibration of a homogeneous beam with a single delamination subjected to axial loads and static end moments", *Acta Mechanica Sinica*, **30**, 607–614. https://doi.org/10.1007/s10409-014-0039-4.

Liu, Y., Xiao, J. and Shu, D. (2014), "Free Vibration of Delaminated Beams with an Edge Crack", *Procedia Eng.*, **75**, 78-82. https://doi.org/10.1016/j.proeng.2013.11.016.

Meirovitch, L. and Silverberg, L.M. (1984), "Active vibration suppression of a cantilever wing", *J. Sound Vib.*, **97**(3), 489-498. https://doi.org/10.1016/0022-460X(84)90274-8.

Minguet, P.J. (1989), "Static and dynamic behaviour of composite helicopter rotor blades under large deflections", Ph.D. Dissertation, Massachusetts Institute of Technology, Massachusetts. http://hdl.handle.net/1721.1/40146.

Mujumdar, P.M. and Suryanarayan, S. (1988), "Flexural vibrations of beams with delaminations", J. *Sound Vib.*, **125**(3), 441-461.https://doi.org/10.1016/0022-460X(88)90253-2.

Shen, M.H.H. and Grady J.E. (1992), "Free vibrations of delaminated beams", *AIAA J.*, **30**(5), 1361-1370. https://doi.org/10.2514/3.11072.

Shiau, L.C. (1992), "Flutter of composite laminated beam plates with delamination", *AIAA J.*, **30(**10**)**, 2504-2511. https://doi.org/10.2514/3.11253.

Shu, D. and Della C.N. (2004), "Free vibration analysis of composite beams with two non-overlapping delaminations", *Int. J. Mech. Sci.*, **46**(4), 509-526. https://doi.org/10.1016/j.ijmecsci.2004.05.008.

Song, O. and Librescu, L. (1991), "Free vibration and aero-elastic divergence of aircraft wings modelled as composite thin-walled beams", *Proceedings of the 32nd Structures, Structural Dynamics, and Materials Conference*, Baltimore, MD, U.S.A., April. https://doi.org/10.2514/6.1991-1187.

Song, O., Ha, T. and Librescu, L. (2003), "Dynamics of anisotropic composite cantilevers weakened by multiple transverse open cracks", *Eng. Fract. Mech.*, **70**(1), 105-123. https://doi.org/10.1016/S0013-7944(02)00022-X.

Sousa, K., Domingues, A.C., Pereira, P., Carneiro, S.H., Morais, M.V. and Fabro, A.T. (2016) "Modal parameter determination of a lightweight aerospace panel using laser doppler vibrometer measurements''. *In AIP Conference Proceedings (Vol. 1740, No. 1, p. 070006).* Ancona, Italy, June. https://doi.org/10.1063/1.4952683.

Strganac, T.W. and Kim, Y. (1996), "Aeroelastic behavior of composite plates subject to damage growth", *J. Aircraft*, **33**(1), 68-73. https://doi.org/10.2514/3.46904.

Wang, K. (2004), "Vibration analysis of cracked composite bending-torsion beams for damage diagnosis", Ph.D. Dissertation, Virginia Polytechnic Institute and State University, Virginia. http://hdl.handle.net/10919/29891.

Wang, K. and Inman, D. (2007), "Crack-induced effects on aero-elasticity of an un-swept composite wing", *AIAA J.*, **45**(3), 542-551. https://doi.org/10.2514/1.21689.

Wang, K., Inman, D.J. and Farrar, C.R. (2005), "Crack-induced changes in divergence and flutter of cantilevered composite panels", *Struct. Health Monit.*, **4**(4), 377-392. https://doi.org/10.1177/1475921705057977.

Weisshaar, T.A. and Foist, B.L. (1985), "Vibration tailoring of advanced composite lifting surfaces", *J. Aircraft*, **22**(2), 141-147. https://doi.org/10.2514/3.45098.

Worden, K. and Barton, J.M.D. (2004), "An overview of intelligent fault detection in systems and structures", *Struct. Health Monit.*, **3**(1), 85-98. https://doi.org/10.1177/1475921704041866.

CC

Appendix A

Nomenclature

L	= span length
b	= chord length
t	= thickness
m	= mass per unit span
a	= crack length
θ	= fiber angle
1,2	= principle axes
x_α	= distance between the mass and elastic axes
$\mathrm{h}(y,t)$	= bending displacement
$\psi(y,t)$	= torsional displacement about the elastic axes
EI	= bending stiffness
GJ	= torsional stiffness
K	= bending–torsion coupling rigidity
I_α	= moment of inertia about the elastic axis
$\xi = y/L$	= crack location ratio (c.l.r)
$eta = \mathrm{a}/b$	= crack depth ratio
ω	= frequency (rad/s)
$\mathrm{H}(y)$	= bending mode shape
$\Psi(y)$	= torsional mode shape
D	= differential operator
$\Theta(\xi)$	= cross-sectional rotation
$\mathrm{M}(\xi)$	= bending moment at any cross section
$\mathrm{S}(\xi)$	= shear force at any cross section
$\mathrm{T}(\xi)$	= torsional moment at any cross section
c_{ij}	= coefficients of local flexibility matrix
$[C]$	= flexibility matrix
$\mathrm{F_{III}}$	= correction factor for third mode of crack
$\mathrm{F_I}$	= correction factor for first mode of crack
$\bar{A}_{ij}$	= compliance matrix components
$\boldsymbol{\Lambda}$	= dynamic stiffness matrix
a	= crack area (crack length for two-dimensional problems)
α, β, γ	= roots of auxiliary equation
A_i, B_i, C_i	= constant coefficients of mode shapes
μ_1,μ_2	= roots of the characteristic equation
Ψ	= coupling parameter
A_{ij}	= constants from compliance elements of the composite along the principle axes
$E_{11}, E_{22}, G_{23}, G_{12}, \nu_{12}, \nu_{21}$	= mechanical properties of the composite
w.r.t	= with regard to

Appendix B

Coefficients $\hat{a}$, $\hat{b}$ and $\hat{c}$ from Eq. (7)

$$\hat{a}=\frac{I_\alpha\omega^2\frac{EI}{L^4}}{\frac{EI.GJ}{L^6}-\frac{K^2}{L^6}}=\frac{I_\alpha\omega^2\frac{EI}{L^4}}{\frac{EI.GJ-K^2}{L^6}}=\frac{I_\alpha\omega^2EIL^2}{EI.GJ-K^2}=\frac{I_\alpha\omega^2EIL^2/EI.GJ}{\left(1-\frac{K^2}{EI.GJ}\right)}=\frac{\bar{a}}{1-k_m} \tag{B-1}$$

$$\hat{b}=\frac{m\omega^2\frac{GJ}{L^2}}{\frac{EI.GJ}{L^6}-\frac{K^2}{L^6}}=\frac{m\omega^2GJL^4}{EI.GJ-K^2}=\frac{\frac{m\omega^2GJL^4}{EI.GJ}}{\left(1-\frac{K^2}{EI.GJ}\right)}=\frac{\bar{b}}{1-k_m} \tag{B-2}$$

$$\hat{b}\hat{c}=-\frac{m^2x_\alpha^2\omega^4-mI_\alpha\omega^4}{\frac{EI.GJ}{L^6}-\frac{K^2}{L^6}}\rightarrow\left(\frac{I_\alpha\omega^2EIL^2}{EI.GJ-K^2}\right)\left(\frac{m\omega^2GJL^4}{EI.GJ-K^2}\right)\hat{c}=-\frac{L^6(m^2x_\alpha^2\omega^4-mI_\alpha\omega^4)}{EI.GJ-K^2}\rightarrow$$
$$\hat{c}=-\frac{mx_\alpha^2}{I_\alpha}+\frac{mK^2x_\alpha^2}{I_\alpha EI.GJ}+1-\frac{K^2}{EI.GJ}=\left(1-\frac{mx_\alpha^2}{I_\alpha}\right)\left(1-\frac{K^2}{EI.GJ}\right)=(1-k_g)(1-k_m) \tag{B-3}$$

Appendix C

Closed form solution of the auxiliary equation Eq. (7) assuming trail solution $W=e^{p\xi}$ will be as

$$p^6+\hat{a}p^4-\hat{b}p^2-\hat{a}\hat{b}\hat{c}=0, \tag{C-1}$$
$$\xrightarrow{\lambda=p^2}\lambda^3+\hat{a}\lambda^2-\hat{b}\lambda-\hat{a}\hat{b}\hat{c}=0\rightarrow\lambda^3+\frac{3\hat{a}}{3}\lambda^2+\left(\frac{\hat{a}^2}{3}-\frac{\hat{a}^2}{3}-\hat{b}\right)\lambda-\hat{a}\hat{b}\hat{c}+\left(\frac{\hat{a}\hat{b}}{3}-\frac{\hat{a}\hat{b}}{3}+\frac{3\hat{a}^3}{27}-\frac{\hat{a}^3}{9}\right)=0$$

$$\begin{cases} q=\hat{b}+\frac{\hat{a}^2}{3} \\ x=\lambda+\frac{\hat{a}}{3} \\ r=\hat{a}\left(\hat{b}\hat{c}-\frac{\hat{b}}{3}-\frac{2\hat{a}^2}{27}\right)\end{cases}\rightarrow x^3-qx-r=0. \tag{C-2}$$

all three roots of equation $x^3-qx-r=0$ as given by Wang (2004) will be as

$$x_1=2\sqrt{q/3}\cos(\phi/3), x_2=2\sqrt{q/3}\cos((\pi-\phi)/3), x_3=2\sqrt{q/3}\cos((\pi-\phi)/3). \tag{C-3}$$

Finally, all six roots of auxiliary equation (Eq (7)) will be defined by parameters α,β,γ,q and ϕ from Eq. (8) as

$$\begin{cases} \alpha^2=2\sqrt{q/3}\cos(\phi/3)-\frac{\hat{a}}{3}\rightarrow(\alpha,-\alpha), \\ \beta^2=2\sqrt{q/3}\cos((\pi-\phi)/3)+\frac{\hat{a}}{3}\rightarrow(i\beta,-i\beta), \\ \gamma^2=2\sqrt{q/3}\cos((\pi+\phi)/3)+\frac{\hat{a}}{3}\rightarrow(i\gamma,-i\gamma)\end{cases} \tag{C-4}$$

$$\cos(\phi)=\frac{27\hat{a}\hat{b}\hat{c}-9\hat{a}\hat{b}-2\hat{a}^3}{2\left(3\hat{b}+\hat{a}^2\right)^{3/2}}, q=\hat{a}+\frac{\hat{b}^2}{3} \tag{C-5}$$

Appendix D

The coefficient θ_i, S_i, M_i and T_i (i=1–6) can be written as follows

$$\Theta_1 = \frac{1}{L}\alpha\, sinh\, \alpha\xi\,, \Theta_2 = \frac{1}{L}\alpha\, cosh\, \alpha\xi\,, \Theta_3 = -\frac{1}{L}\beta\, sin\, \beta\xi,$$
$$\Theta_4 = \frac{1}{L}\beta\, cos\, \beta\xi\,, \Theta_5 = -\frac{1}{L}\gamma\, sin\, \gamma\xi\,, \Theta_6 = \frac{1}{L}\gamma\, cos\, \gamma\xi, \tag{D-1}$$

$$T_1 = \left(-\frac{K}{L^2}\alpha^2 \cosh \alpha\xi + \frac{GJ}{L}\frac{e_\alpha g_\alpha}{L}\alpha \sinh \alpha\xi - \frac{GJ}{L}\frac{e_\alpha}{L}\alpha \cosh \alpha\xi\right),$$

$$T_2 = \left(-\frac{K}{L^2}\alpha^2 \sinh \alpha\xi - \frac{GJ}{L}\frac{e_\alpha}{L}\alpha \sinh \alpha\xi + \frac{GJ}{L}\frac{e_\alpha g_\alpha}{L}\alpha \cosh \alpha\xi\right),$$

$$T_3 = \left(\frac{K}{L^2}\beta^2 \cos \beta\xi + \frac{GJ}{L}\frac{e_\beta g_\beta}{L}\beta \sin \beta\xi + \frac{GJ}{L}\frac{e_\beta}{L}\beta \cos \beta\xi\right),$$

$$T_4 = \left(\frac{K}{L^2}\beta^3 \sin \beta\xi + \frac{GJ}{L}\frac{e_\beta}{L}\beta \sin \beta\xi - \frac{GJ}{L}\frac{e_\beta g_\beta}{L}\beta \cos \beta\xi\right), \tag{D-2}$$

$$T_5 = \left(\frac{K}{L^2}\gamma^2 \cos \gamma\xi + \frac{GJ}{L}\frac{e_\gamma g_\gamma}{L}\gamma \sin \gamma\xi + \frac{GJ}{L}\frac{e_\gamma}{L}\gamma \cos \gamma\xi\right),$$

$$T_6 = \left(\frac{K}{L^2}\gamma^2 \sin \gamma\xi + \frac{GJ}{L}\frac{e_\gamma}{L}\gamma \sin \gamma\xi - \frac{GJ}{L}\frac{e_\gamma g_\gamma}{L}\gamma \cos \gamma\xi\right).$$

$$S_1 = \left(\frac{EI}{L^3}\alpha^3 \sinh \alpha\xi - \frac{K}{L^2}\frac{e_\alpha g_\alpha}{L}\alpha^2 \cosh \alpha\xi + \frac{K}{L^2}\frac{e_\alpha}{L}\alpha^2 \sinh \alpha\xi\right),$$

$$S_2 = \left(\frac{EI}{L^3}\alpha^3 \cosh \alpha\xi + \frac{K}{L^2}\frac{e_\alpha}{L}\alpha^2 \cosh \alpha\xi - \frac{K}{L^2}\frac{e_\alpha g_\alpha}{L}\alpha^2 \sinh \alpha\xi\right),$$

$$S_3 = \left(\frac{EI}{L^3}\beta^3 \sin \beta\xi - \frac{K}{L^2}\frac{e_\beta g_\beta}{L}\beta^2 \cos \beta\xi + \frac{K}{L^2}\frac{e_\beta}{L}\beta^2 \sin \beta\xi\right),$$

$$S_4 = \left(-\frac{EI}{L^3}\beta^3 \cos \beta\xi - \frac{K}{L^2}\frac{e_\beta}{L}\beta^2 \cos \beta\xi - \frac{K}{L^2}\frac{e_\beta g_\beta}{L}\beta^2 \sin \beta\xi\right), \tag{D-3}$$

$$S_5 = \left(\frac{EI}{L^3}\gamma^3 \sin \gamma\xi - \frac{K}{L^2}\frac{e_\gamma g_\gamma}{L}\gamma^2 \cos \gamma\xi + \frac{K}{L^2}\frac{e_\gamma}{L}\gamma^2 \sin \gamma\xi\right),$$

$$S_6 = \left(-\frac{EI}{L^3}\gamma^3 \cos \gamma\xi - \frac{K}{L^2}\frac{e_\gamma}{L}\gamma^2 \cos \gamma\xi - \frac{K}{L^2}\frac{e_\gamma g_\gamma}{L}\gamma^2 \sin \gamma\xi\right),$$

$$M_1 = \left(-\frac{EI}{L^2}\alpha^2 \cosh \alpha\xi + \frac{K}{L}\frac{e_\alpha g_\alpha}{L}\alpha \sinh \alpha\xi - \frac{K}{L}\frac{e_\alpha}{L}\alpha \cosh \alpha\xi\right),$$

$$M_2 = \left(-\frac{EI}{L^2}\alpha^2 \sinh \alpha\xi - \frac{K}{L}\frac{e_\alpha}{L}\alpha \sinh \alpha\xi + \frac{K}{L}\frac{e_\alpha g_\alpha}{L}\alpha \cosh \alpha\xi\right),$$

$$M_3 = \left(\frac{EI}{L^2}\beta^2 \cos \beta\xi + \frac{K}{L}\frac{e_\beta g_\beta}{L}\beta \sin \beta\xi + \frac{K}{L}\frac{e_\beta}{L}\beta \cos \beta\xi\right),$$

$$M_4 = \left(\frac{EI}{L^2}\beta^2 \sin \beta\xi + \frac{K}{L}\frac{e_\beta}{L}\beta \sin \beta\xi - \frac{K}{L}\frac{e_\beta g_\beta}{L}\beta \cos \beta\xi\right), \tag{D-4}$$

$$M_5 = \left(\frac{EI}{L^2}\gamma^2 \cos \gamma\xi + \frac{K}{L}\frac{e_\gamma g_\gamma}{L}\gamma \sin \gamma\xi + \frac{K}{L}\frac{e_\gamma}{L}\gamma \cos \gamma\xi\right),$$

$$M_6 = \left(\frac{EI}{L^2}\gamma^2 \sin \gamma\xi + \frac{K}{L}\frac{e_\gamma}{L}\gamma \sin \gamma\xi - \frac{K}{L}\frac{e_\gamma g_\gamma}{L}\gamma \cos \gamma\xi\right).$$

Appendix E

Local flexibility matrix coefficients from Eq. (34)

$$c_{26}=c_{62}=\frac{96\pi^3 D_3 b}{(\pi^5 bt^2-192t^3)}\Lambda_{III}, c_{22}=\frac{2\pi D_3}{t}\Lambda_{III},$$
$$c_{66}=\frac{576 D_3\pi^7 b^2 t}{(\pi^5 bt^2-192t^3)^2}\Lambda_{III}, c_{44}=\frac{24\pi D_1 Y_I^2}{t}\Lambda_I \tag{E-1}$$

$$\Lambda_{III}=\frac{1}{b^2}\int_0^{\mathrm{a}} a[\mathrm{F_{III}}(a/b)]^2 da \xrightarrow{\bar{\alpha}=\frac{a}{b},\bar{a}=\frac{\mathrm{a}}{b}} \Lambda_{III}=\int_0^{\bar{a}} \bar{\alpha}[\mathrm{F_{III}}(\bar{\alpha})]^2 d\bar{\alpha}, \tag{E-2}$$

$$\Lambda_I=\frac{1}{b^2}\int_0^{\mathrm{a}} a[\mathrm{F_I}(a/b)]^2 d\alpha=\int_0^{\bar{a}} \bar{\alpha}[\mathrm{F_I}(\bar{\alpha})]^2 d\bar{\alpha} \tag{E-3}$$

Where, $\mathrm{F_{III}}$ denote correction factor for third mode of crack and defined as

$$\mathrm{F_{III}}\left(\frac{a}{b}\right)=\sqrt{\frac{\tan\lambda}{\lambda}}, \lambda=\frac{\pi \mathrm{a}}{2b}, \tag{E-4}$$

$$\Lambda_{III}=-\frac{4}{\pi^2}\ln\left(\cos\frac{\mathrm{a}}{b}\right) \tag{E-5}$$

And F_I denote the correction factor for first mode of crack and is defined as

$$\mathrm{F_I}(\bar{\alpha})=\sqrt{\frac{\tan\lambda}{\lambda}}\frac{[0.752+2.02(a/b)+0.37(1-\sin\lambda)^3]}{\cos\lambda} \tag{E-6}$$

Constants D_1, D_2, D_3 and D_{12} are defined as

$$D_1=-\frac{\bar{A}_{22}}{2}Im\left(\frac{\mu_1+\mu_2}{\mu_1\mu_2}\right),$$
$$D_2=\frac{\bar{A}_{11}}{2}Im(\mu_1+\mu_2), D_{12}=\bar{A}_{11}Im(\mu_1\mu_2), D_3=\frac{1}{2}\sqrt{A_{44}A_{55}}. \tag{E-7}$$

In which μ_1 and μ_2 are positive imaginary parts of characteristics equation roots

$$\bar{A}_{11}\mu^4-2\bar{A}_{16}\mu^3+(2\bar{A}_{12}+\bar{A}_{66})\mu^2-2\bar{A}_{26}\mu+\bar{A}_{22}=0, \tag{E-8}$$

Compliance matrix components are

$$\bar{A}_{11}=A_{11}m^4+(2A_{12}+A_{66})m^2n^2+A_{22}n^4,$$
$$\bar{A}_{22}=A_{11}n^4+(2A_{12}+A_{66})m^2n^2+A_{22}m^4,$$
$$\bar{A}_{12}=(A_{11}+A_{22}-A_{66})m^2n^2+A_{12}(m^4+n^4),$$
$$\bar{A}_{16}=(2A_{11}+2A_{12}-A_{66})m^3n-(2A_{22}-2A_{12}-A_{66})mn^3,$$
$$\bar{A}_{26}=(2A_{11}-2A_{12}-A_{66})mn^3-(2A_{22}-2A_{12}-A_{66})m^3n,$$
$$\bar{A}_{66}=2(2A_{11}+2A_{22}-4A_{12}-A_{66})m^2n^2+A_{66}(m^4+n^4), \tag{E-9}$$

With $m=\cos\theta$, $n=sin\,\theta$ and θ is fiber angle. Constants A_{11}, A_{22}, A_{66} and A_{12} for plane stress condition are

$$A_{11}=\frac{1}{E_{11}}, A_{22}=\frac{1}{E_{22}}, A_{12}=-\frac{\nu_{12}}{E_{11}}=-\frac{\nu_{21}}{E_{22}}, A_{44}=\frac{1}{G_{23}}, A_{55}=A_{66}=\frac{1}{G_{12}}. \tag{E-10}$$

Appendix F

To find the relationships between the coefficients $A_{1-6}$and B_{1-6}, substitute Eq. (9) to the first of Eq. (1)

$$\begin{aligned}&\overbrace{\left(\frac{EI}{L^4}A_1\alpha^4+\frac{K}{L^3}B_2\alpha^3-m\omega^2A_1+mx_\alpha\omega^2B_1\right)}^{(F1)}\cosh\alpha\xi\\&+\overbrace{\left(\frac{EI}{L^4}A_2\alpha^4+\frac{K}{L^3}B_1\alpha^3-m\omega^2A_2+mx_\alpha\omega^2B_2\right)}^{(F2)}\sinh\alpha\xi\\&+\overbrace{\left(\frac{EI}{L^4}A_3\beta^4-\frac{K}{L^3}B_4\beta^3-m\omega^2A_3+mx_\alpha\omega^2B_3\right)}^{(F3)}\cos\beta\xi\\&+\overbrace{\left(\frac{EI}{L^4}A_4\beta^4+\frac{K}{L^3}B_3\beta^3-m\omega^2A_4+mx_\alpha\omega^2B_4\right)}^{(F4)}\sin\beta\xi\\&+\overbrace{\left(\frac{EI}{L^4}A_5\gamma^4-\frac{K}{L^3}B_6\gamma^3-m\omega^2A_5+mx_\alpha\omega^2B_5\right)}^{(F5)}\cos\gamma\xi\\&+\overbrace{\left(\frac{EI}{L^4}A_6\gamma^4+\frac{K}{L^3}B_5\gamma^3-m\omega^2A_6+mx_\alpha\omega^2B_6\right)}^{(F6)}\sin\gamma\xi=0\end{aligned}\tag{F-1}$$

from the equation $(F1)$ of the equation (F-1), B_1 is derived as

$$\begin{aligned}&\frac{EI}{L^4}A_1\alpha^4+\frac{K}{L^3}B_2\alpha^3-m\omega^2A_1+mx_\alpha\omega^2B_1=0\rightarrow\\&B_1=-\frac{EI}{mx_\alpha\omega^2L^4}A_1\alpha^4-\frac{K}{mx_\alpha\omega^2L^3}B_2\alpha^3+\frac{1}{x_\alpha}A_1,\end{aligned}\tag{F-2}$$

then B_1 is substituted in the Eq. (2)

$$\begin{aligned}&\frac{EI}{L^4}A_2\alpha^4+\frac{K}{L^3}B_1\alpha^3-m\omega^2A_2+mx_\alpha\omega^2B_2=0\rightarrow\\&\frac{EI}{L^4}A_2\alpha^4+\frac{K}{L^3}\left(-\frac{EI}{mx_\alpha\omega^2L^4}A_1\alpha^4-\frac{K}{mx_\alpha\omega^2L^3}B_2\alpha^3+\frac{1}{x_\alpha}A_1\right)\alpha^3\\&-m\omega^2A_2+mx_\alpha\omega^2B_2=0\rightarrow\\&\left(-\frac{K^2}{mx_\alpha\omega^2L^6}\alpha^6+mx_\alpha\omega^2\right)B_2=\left(\frac{EIK}{mx_\alpha\omega^2L^7}\alpha^7-\frac{K}{x_\alpha L^3}\alpha^3\right)A_1+\left(-\frac{EI}{L^4}\alpha^4+m\omega^2\right)A_2\end{aligned}\tag{F-3}$$

finally, after an algebraic manipulation B_2 is derived as

$$B_2=\frac{\left(\frac{EIK}{mx_\alpha\omega^2L^7}\alpha^7-\frac{K}{x_\alpha L^3}\alpha^3\right)}{\left(-\frac{K^2}{mx_\alpha\omega^2L^6}\alpha^6+mx_\alpha\omega^2\right)}A_1+\frac{\left(-\frac{EI}{L^4}\alpha^4+m\omega^2\right)}{\left(-\frac{K^2}{mx_\alpha\omega^2L^6}\alpha^6+mx_\alpha\omega^2\right)}A_2=\frac{e_\alpha}{L}A_1-\frac{e_\alpha g_\alpha}{L}A_2\tag{F-4}$$

B_2 is substituted in the Eq. (2) and after an algebraic manipulation B_1 is derived a

$$B_1=-\frac{e_\alpha g_\alpha}{L}A_1+\frac{e_\alpha}{L}A_2.\tag{F-5}$$

In the same manner, other relationships between coefficients A_{1-6} and B_{1-6} are obtained as

$$\begin{aligned}
&\xrightarrow{from\ (1),(2)} B_1 = -\frac{e_\alpha g_\alpha}{L}A_1 + \frac{e_\alpha}{L}A_2, B_2 = \frac{e_\alpha}{L}A_1 - \frac{e_\alpha g_\alpha}{L}A_2,\\
&\xrightarrow{from\ (3),(4)} B_3 = -\frac{e_\beta g_\beta}{L}A_3 + \frac{e_\beta}{L}A_4, B_4 = -\frac{e_\beta}{L}A_3 + \frac{e_\beta g_\beta}{L}A_4,\\
&\xrightarrow{from\ (5),(6)} B_5 = \frac{e_\gamma g_\gamma}{L}A_5 + \frac{e_\gamma}{L}A_6, B_6 = -\frac{e_\gamma}{L}A_5 + \frac{e_\gamma g_\gamma}{L}A_6.
\end{aligned} \tag{F-6}$$

For sample, algebraic manipulation for the first expression of the equation (F-4) will be as (F-7) and for the second expression of the equation (F-4) will be as (F-8).

$$\begin{aligned}
&\frac{\left(\frac{EIK}{mx_\alpha\omega^2L^7}\alpha^7 - \frac{K}{x_\alpha L^3}\alpha^3\right)}{\left(-\frac{K^2}{mx_\alpha\omega^2L^6}\alpha^6 + mx_\alpha\omega^2\right)} = \frac{\frac{EIK\alpha^7 - m\omega^2L^4K\alpha^3}{mx_\alpha\omega^2L^7}}{\frac{-K^2\alpha^6 + m^2{x_\alpha}^2\omega^4L^6}{mx_\alpha\omega^2L^6}} = \frac{-EIK\alpha^7 + m\omega^2L^4K\alpha^3}{LK^2\alpha^6 - m^2{x_\alpha}^2\omega^4L^7}\\
&= \frac{\alpha^3(-EIK\alpha^4 + m\omega^2L^4K)}{LK^2\alpha^6 - m^2{x_\alpha}^2\omega^4L^7} \xrightarrow{\times\frac{L}{L}}\\
&= \frac{\alpha^3(-EIKL\alpha^4 + m\omega^2L^5K)}{L^2K^2\alpha^6 - m^2{x_\alpha}^2\omega^4L^8} = LK\frac{\alpha^3(-EI\alpha^4 + m\omega^2L^4)}{L^2K^2\alpha^6 - m^2{x_\alpha}^2\omega^4L^8} \xrightarrow{\times\frac{(EILK)^2}{(EILK)^2}} \frac{\alpha^3(EILK)^2(-EI\alpha^4 + m\omega^2L^4)}{(EILK)^2(L^2K^2\alpha^6 - m^2{x_\alpha}^2\omega^4L^8)} =
\end{aligned}$$

$$\begin{aligned}
&LK\frac{\alpha^3(EILK)^2(-EI\alpha^4 + m\omega^2L^4)}{(EILK)^2(L^2K^2\alpha^6 - m^2{x_\alpha}^2\omega^4L^8)} = \frac{EI}{LK}\left(\frac{\alpha^3\left(\frac{-EI\alpha^4 + m\omega^2L^4}{EI}\right)}{\frac{(EIKL)^2\alpha^6 - m^2{x_\alpha}^2\omega^4L^8(EI)^2}{(EILK)^2}}\right)\\
&= \frac{EI}{LK}\left(\frac{\alpha^3\left(\frac{-EI\alpha^4 + m\omega^2L^4}{EI}\right)}{\alpha^6 - \frac{m^2{x_\alpha}^2\omega^4L^8(EI)^2}{(EILK)^2}}\right) \xrightarrow{\times\frac{\alpha^6}{\alpha^6}} \frac{EI}{LK}\left(\frac{\frac{\alpha^3\left(\frac{m\omega^2L^4}{EI} - \alpha^4\right)}{\alpha^6}}{\frac{\alpha^6 - \frac{m^2{x_\alpha}^2\omega^4L^8(EI)^2}{(EILK)^2}}{\alpha^6}}\right)\\
&= \frac{EI}{LK}\left(\frac{\frac{\left(\frac{m\omega^2L^4}{EI} - \alpha^4\right)}{\alpha^3}}{\frac{\alpha^6 - \frac{m^2\omega^4L^8}{(EI)^2}\frac{{x_\alpha}^2}{L^2}\left(\frac{EI}{K}\right)^2}{\alpha^6}}\right) \xrightarrow{\frac{m\omega^2L^4}{EI}=\bar{b}} = \frac{1}{L}\left(\frac{\frac{EI}{K}\left(\bar{b} - \alpha^4\right)}{\frac{\alpha^3}{1 - \frac{\bar{b}^2\left(\frac{x_\alpha}{L}\frac{EI}{K}\right)^2}{\alpha^6}}}\right) \xrightarrow{\frac{EI}{K}(\bar{b}-\alpha^4)=k_\alpha,\frac{x_\alpha EI}{L\ K}=k_\delta}\\
&= \frac{1}{L}\left(\frac{k_\alpha}{1 - \frac{\bar{b}^2{k_\delta}^2}{\alpha^6}}\right) = \frac{1}{L}\left(\frac{k_\alpha}{1 - \left(\frac{\bar{b}k_\delta}{\alpha^3}\right)^2}\right) \xrightarrow{\frac{\bar{b}k_\delta}{\alpha^3}=g_\alpha} = \frac{1}{L}\left(\frac{k_\alpha}{1 - {g_\alpha}^2}\right) = \frac{e_\alpha}{L}.
\end{aligned} \tag{F-7}$$

$$\frac{\left(-\frac{EI}{L^4}\alpha^4+m\omega^2\right)}{\left(-\frac{K^2}{mx_\alpha\omega^2L^6}\alpha^6+mx_\alpha\omega^2\right)}=\frac{\frac{EI\alpha^4-m\omega^2L^4}{L^4}}{\frac{K^2\alpha^6-m^2{x_\alpha}^2\omega^4L^6}{mx_\alpha\omega^2L^6}}=\frac{mx_\alpha\omega^2L^2(EI\alpha^4-m\omega^2L^4)}{K^2\alpha^6-m^2{x_\alpha}^2\omega^4L^6}$$

$$=-\frac{mx_\alpha\omega^2L^4(m\omega^2L^4-EI\alpha^4)}{L^2(K^2\alpha^6-m^2{x_\alpha}^2\omega^4L^6)}=$$

$$-\frac{EI^2(m^2x_\alpha\omega^4L^8-mx_\alpha\omega^2L^4\alpha^4EI)}{EI^2(K^2L^2\alpha^6-m^2{x_\alpha}^2\omega^4L^8)}=-\frac{EI(m^2x_\alpha\omega^4L^8EI-mx_\alpha\omega^2L^4\alpha^4EI^2)}{(KLEI)^2\alpha^6-m^2{x_\alpha}^2\omega^4L^8EI^2}$$

$$=-\frac{\frac{m^2x_\alpha\omega^4L^8EI-mx_\alpha\omega^2L^4\alpha^4EI^2}{1}}{\frac{(KLEI)^2\alpha^6-m^2{x_\alpha}^2\omega^4L^8EI^2}{EI}}\xrightarrow{\times\frac{EILK^2}{EILK^2}}$$

$$-\frac{\frac{m^2x_\alpha\omega^4L^8EI-mx_\alpha\omega^2L^4\alpha^4EI^2}{EILK^2}}{L\left(\frac{(KLEI)^2\alpha^6-m^2{x_\alpha}^2\omega^4L^8EI^2}{EIL^2K^2}\right)}=-\frac{\frac{m^2x_\alpha\omega^4L^8}{LK^2}-\frac{m\omega^2L^4}{EI}\left(\frac{EI}{K}\right)^2\frac{x_\alpha}{L}\alpha^4}{L\left(\frac{(EILK)^2\alpha^6-m^2{x_\alpha}^2\omega^4L^8EI^2}{(EILK)^2}\right)}$$

$$=-\frac{\frac{m\omega^2L^4}{EI}\left(\frac{EI}{K}\right)^2\frac{x_\alpha}{L}\left(\frac{m\omega^2L^4}{EI}-\alpha^4\right)}{L\left(\alpha^6-\left(\frac{m\omega^2L^4}{EI}\right)^2\left(\frac{x_\alpha}{L}\right)^2\left(\frac{EI}{K}\right)^2\right)}\xrightarrow{\times\frac{\alpha^6}{\alpha^6}}=-\frac{\frac{\frac{m\omega^2L^4}{EI}\left(\frac{EI}{K}\right)^2\frac{x_\alpha}{L}\left(\frac{m\omega^2L^4}{EI}-\alpha^4\right)}{\alpha^6}}{L\left(\frac{\alpha^6-\left(\frac{m\omega^2L^4}{EI}\right)^2\left(\frac{x_\alpha}{L}\right)^2\left(\frac{EI}{K}\right)^2}{\alpha^6}\right)} \tag{F-8}$$

$$=-\frac{\frac{m\omega^2L^4}{EI}\frac{EI}{K}\frac{x_\alpha}{L}}{L\left(1-\left(\frac{\frac{m\omega^2L^4}{EI}\frac{EI}{K}\frac{x_\alpha}{L}}{\alpha^3}\right)^2\right)}\times\frac{\frac{EI}{K}\left(\frac{m\omega^2L^4}{EI}-\alpha^4\right)}{\alpha^3}=-\frac{\frac{\bar{b}k_\delta}{\alpha^3}k_\alpha}{L\left(1-\left(\frac{\bar{b}k_\delta}{\alpha^3}\right)^2\right)}=-\frac{g_\alpha k_\alpha}{L(1-g_\alpha^2)}$$

$$=-\frac{\frac{g_\alpha k_\alpha}{(1-g_\alpha^2)}}{L}=-\frac{e_\alpha g_\alpha}{L}.$$